6420 *Biochemistry* **2010,** *49,* 6420–6429
DOI: 10.1021/bi100489x

BIOCHEMISTRY
including biophysical chemistry & molecular biology
Article

The N-Terminal Integrity Is Critical for the Stability and Biological Functions of Endostatin[†]

Yan Fu and Yongzhang Luo*

National Engineering Laboratory for Anti-tumor Protein Therapeutics, Beijing Key Laboratory of Protein Therapeutics, and Cancer Biology Laboratory, School of Life Sciences, Tsinghua University, Beijing 100084, P. R. China

Received April 1, 2010; Revised Manuscript Received June 10, 2010

ABSTRACT: Endostatin is an endogenous angiogenesis inhibitor, and amino acid residues H1, H3, H11, and D76 at its N-terminus coordinate with one zinc ion. Recombinant endostatin suffering from N-terminal truncations during *Pichia pastoris* expression was widely used in previous studies and generated inconsistent antitumor results. However, little attention was paid to the possible alteration on the stability and activity of endostatin caused by N-terminal truncations. In this study, N-terminally truncated forms of endostatin expressed by *P. pastoris* are identified as N-1, N-3, and N-4, in which one or two of the four zinc-binding residues are lost. The N-terminal truncation of the first amino acid residue (H) does not result in a significant change in the conformation, zinc-binding capacity, thermodynamic stability, or biological activity, while truncations of the first three amino acid residues (HSH) or the first four amino acid residues (HSHR) dramatically decrease the thermodynamic stability measured by urea-induced unfolding and biological activities of endostatin both *in vitro* and *in vivo*. Intriguingly, ZBP-endostatin with a short extra zinc-binding peptide (ZBP) engineered at the N-terminus exhibits a more tightly packed tertiary structure and increased thermodynamic stability and cooperativity against urea, with more potent antiendothelial and antitumor activities than the wild-type endostatin. These findings demonstrate that the N-terminal integrity is essential for the stability and biological functions of endostatin, which provides fundamental explanations for the inconsistent antitumor activities of endostatin in a variety of studies, including the different therapeutic efficacies of endostatin and ZBP-endostatin in clinical trials.

Endostatin, a 20 kDa carboxyl-terminal fragment of collagen XVIII, is an endogenous angiogenesis inhibitor (*1*), and its antitumor activity in animal models was first observed with its inclusion body form expressed by *Escherichia coli* (*1*). To avoid the refolding problem, *Pichia pastoris* had to be widely employed for soluble recombinant endostatin expression in many previous studies, including the clinical trials performed in the United States (*2*−*5*). Since N-terminal truncation is a common phenomenon in proteins expressed by *P. pastoris*, the N-terminally truncated endostatin expressed by yeast has been observed and well accepted so far (*2*, *3*). Although discrepant observations about the antitumor efficacies of endostatin have been reported by different groups in the past 13 years (*1*, *6*−*10*), no attention has been paid to the possible alteration of the stability and biological functions of this protein caused by the N-terminal truncation during *P. pastoris* expression.

Crystal structure analysis has revealed that endostatin has a globular structure with a zinc-binding site at its N-terminus (*11*−*13*). Moreover, critical amino acid residues involved in zinc-binding were identified as H1, H3, H11, and D76, and their contributions to zinc-binding were also characterized (*12*, *13*). It was further demonstrated that zinc-binding increases the thermal and thermodynamic stabilities of endostatin (*14*), while reports on the contributions of zinc-binding to the biological functions of endostatin have remained controversial (*2*, *3*). In addition, a synthetic peptide with 27 amino acid residues corresponding to the N-terminal zinc-binding domain of endostatin was reported to be responsible for the antiangiogenic activity of endostatin (*15*). All these studies imply that the N-terminal fragment is very important for the stability and activity of endostatin. Although the zinc-binding capacity can partially explain the contributions of the N-terminal fragment of endostatin, there is no direct evidence to evaluate whether the N-terminally truncated forms of endostatin expressed by yeast maintains the stability and biological functions of the wild-type endostatin.

Two versions of endostatin have been tested in clinical trials so far but showed discrepant results (*4*, *10*, *16*−*20*). They are the recombinant wild-type human endostatin expressed by *P. pastoris* (pES)[1] and the N-terminally modified recombinant human

[†]This work was supported in part by the National High Technology Research and Development Program of China (2007AA02Z155) and the State Key Development Program for Basic Research of China (2006CB910305).

*To whom correspondence should be addressed. Telephone: 86-10-6277-2897. Fax: 86-10-6279-4691. E-mail: yluo@tsinghua.edu.cn.

[1]Abbreviations: pES, human endostatin expressed in *P. pastoris*; ES, wild-type human endostatin with an intact N-terminus expressed in *E. coli*; N-1, human endostatin mutant lacking the first N-terminal His residue expressed in *E. coli*; N-3, human endostatin mutant lacking the first three amino acid residues (HSH) from the N-terminus expressed in *E. coli*; N-4, human endostatin mutant lacking the first four amino acid residues (HSHR) from the N-terminus expressed in *E. coli*; ZBP-ES, human endostatin derivative with an extra zinc-binding peptide (ZBP) engineered at the N-terminus of the wild-type endostatin expressed in *E. coli*; CD, circular dichroism; FL, Trp emission fluorescence; MALDI TOF MS, matrix-assisted laser desorption ionization time-of-flight mass spectrometry; AUC, analytical ultracentrifuge; DSC, differential scanning calorimetry; HMECs, human microvascular endothelial cells; LLC, Lewis lung carcinoma.

 Published on Web 06/14/2010

endostatin expressed by *E. coli*. This endostatin derivative was engineered *via* addition of an extra zinc-binding peptide (ZBP) to the N-terminus of the wild-type endostatin (ZBP-ES for short). Because pES and ZBP-ES have different N-terminal sequences and were expressed by different expression systems, the exact reason for their different clinical efficacies remains largely unknown.

In this study, each individual variant with different N-terminal truncations in pES was identified and then expressed in *E. coli*, followed by being correctly refolded to their native structures. Parallel comparisons of the wild-type endostatin (ES) and its variants as well as ZBP-ES all the way from *in vitro* biochemical properties to *in vivo* antitumor efficacies were conducted. In this work, ES specifically refers to the wild-type human endostatin expressed by *E. coli* with an intact N-terminus, pES refers to the heterogeneous products of recombinant human endostatin expressed by *P. pastoris*, and ZBP-ES refers to the recombinant human endostatin with an extra zinc-binding peptide (MGGSHHHHH) attached to its N-terminus and expressed by *E. coli*.

We report here that three forms of N-terminal truncations, including N-1, N-3, and N-4, were identified with endostatin expressed by *P. pastoris*, which show impaired zinc-binding capacity, reduced thermodynamic stability measured by urea-induced unfolding, and decreased biological activities when compared with those of ES. Moreover, ZBP-ES shows increased thermodynamic stability in urea-induced unfolding, and more potent antiendothelial and antitumor activities than ES. In addition, the antiangiogenic and antitumor activities of ZBP-ES are significantly more potent than those of pES, which reflects the overall contributions by intact endostatin and its N-terminally truncated variants.

In brief, the N-terminal integrity and zinc-binding capacity are very critical for the structure, stability, and biological functions of endostatin. These results bring novel understanding to the endostatin expressed in *P. pastoris* and provide fundamental explanations for the inconsistent activities of endostatin, especially the different clinical performance of pES and ZBP-ES.

MATERIALS AND METHODS

Proteins, Antibodies, Chemicals, and Cell Lines. Recombinant pES was expressed in *P. pastoris*. Culture medium containing soluble pES was dialyzed against 20 mM NaH_2PO_4 (pH 8.0) before beine run through the SP-Sepharose Fast Flow column (GE Healthcare), which was followed by NaCl gradient elution. Recombinant endostatin lacking the first N-terminal His residue (N-1), lacking the first three amino acid residues (HSH) from the N-terminus (N-3), and lacking the first four amino acid residues (HSHR) from the N-terminus (N-4), wild-type endostatin (ES), and ZBP-ES [with nine extra amino acid residues (MGGSHHHHH) attached to the N-terminus of the wild-type endostatin] were all expressed in *E. coli*. ES and its variants (N-1, N-3, N-4, and ZBP-ES) all formed inclusion bodies upon expression in *E. coli*. These inclusion bodies were dissolved in 20 mM Tris-HCl containing 8 M urea and 10 mM DDT (pH 8.6) and then subjected to a Q-Sepharose High Performance column (GE Healthcare) for purification. Purified denatured and reduced ES proteins (> 95% pure based on HPLC analysis) were subjected to refolding by being slowly dialyzed against 10 mM Tris-HCl (pH 8.0) at 25 °C overnight, and the nonrefolded protein was precipitated by addition of 200 mM NaCl and centrifuged at 12000 rpm and 4 °C. Then the SP-Sepharose Fast Flow column (GE Healthcare) was used for the purification of refolded proteins, and the elution buffer was 20 mM Tris-HCl (pH 8.0) with a 100 to 300 mM NaCl gradient. All purifications were conducted on AKTAprime plus (GE Healthcare), and all protein samples were more than 95% pure.

Apo- and holoproteins were prepared according to the procedure described by Han et al. (*14*) except that 0.9% NaCl was added to 5 mM Tris-HCl to avoid nonspecific binding of zinc ions, and a 20-fold molar excess of $ZnCl_2$ was used for holoprotein preparation.

The mouse anti-ES monoclonal antibody was purchased from Oncogene. Human microvascular endothelial cells (HMECs) are from an HDMEC cell line (catalog no. 2000, Sciencell) transfected with SV40 large T antigen, cultured with DMEM with 10% FBS according to previous reports (*21*−*23*). Lewis lung carcinoma cells were obtained from ATCC.

Identification of Disulfide Bond Patterns. ES, N-1, N-3, N-4, ZBP-ES, and pES were first digested by trypsin (Roche) and chymotrypsin (Sigma). A fraction of digested fragments were reduced by incubation for 1 h with 10 mM DTT at 56 °C, which was followed by a further incubation with 25 mM IAA (*trans*-3-indoleacrylic acid) for 1 h in the dark. The molecular weights of the nonreduced and reduced digested fragments were measured with an AB4700 MALDI TOF/TOF instrument (AB).

Zinc Content Analysis. Holo-ES, holo-N-1, holo-N-3, holo-N-4, and holo-ZBP-ES were prepared as described above. After dialysis, the protein concentration of each sample was determined by the Edelhoch method (*24*). Zinc content was measured by atomic absorption spectroscopy with an OPTIMA 3300RL instrument. An average Zn(II):protein molar ratio was calculated for each protein based on three parallel samples. The dialysis buffer served as a control.

Circular Dichroism (CD) Spectroscopy. Far-UV and near-UV circular dichroism (CD) measurements in the presence of zinc ions were taken on a Jasco-715 spectropolarimeter following the procedure described in our previous study (*25*) with modifications. Briefly, stocks of ES or its variants were diluted in 5 mM Tris-HCl containing 0.9% NaCl (pH 7.4) to a final concentration of 10 μM. All measurements were performed at 37 °C. A 10-fold molar excess of $ZnCl_2$ was added to ensure sufficient zinc-binding.

Tryptophan Emission Fluorescence. Trp emission fluorescence (FL) spectra of ES and ES variants were measured with a Hitachi F-4500 spectrophotometer equipped with a temperature-controlled liquid system as described by Fu et al. (*26*) in the presence of zinc ions. The emission spectra were measured from 300 to 400 nm (excitation and emission slit widths of 10 and 5 nm, respectively) at the excitation wavelength of 288 nm, and the scanning speed was 240 nm/min. The concentrations of all protein samples in 5 mM Tris-HCl containing 0.9% NaCl were 1 μM, and all measurements were taken at 37 °C and pH 7.4. A 10-fold molar excess of $ZnCl_2$ was added to ensure sufficient zinc-binding.

Sedimentation Velocity Analysis. The sedimentation velocity analysis was conducted on a ProteomeLab XL-1 analytical ultracentrifuge (Beckman Coulter) at 60000 rpm and 20 °C. The concentrations of holoprotein samples were around 0.5 mg/mL, and the OD_{280} values were around 0.8. The protein samples were in 5 mM Tris-HCl containing 0.9% NaCl (pH 7.4), and a reference blank containing all reagents except protein was measured as a control. The f/f_0 value of each sample was derived with the software provided by the manufacturer.

Urea-Induced Unfolding of Proteins. Urea-induced unfolding was performed according to the procedures described by Fu et al. (*26*) with modifications. Briefly, the concentrations of holo-ES, holo-N-1, holo-N-3, holo-N-4, and holo-ZBP-ES were 1 μM, and the buffer was 5 mM Tris-HCl (pH 7.4) at 37 °C. A 10-fold molar excess of zinc ions (10 μM $ZnCl_2$) was added to the unfolding system to ensure sufficient zinc-binding of the protein samples, and 0.9% NaCl was also included to mimic the physiological condition and to prevent nonspecific zinc-binding (*26*). Cynate free urea was used, and a reference blank at each concentration of urea containing all reagents except protein was measured for each sample at identical settings, of which the fluorescence spectra were eliminated during data collection. Equilibrations were reached after incubation of the protein samples for 4 h at the indicated urea concentrations.

Urea-induced unfolding curves were fitted and normalized by a two-state model described by the procedure of Santoro and Bolen (*27*), which uses data both inside and outside the transition zone to fix the baselines. The fluorescence data points between 0 and 1 M urea were omitted from the analysis if they show fluorescence increasing with urea concentration (*28*). Superimposed curves were obtained with urea-induced unfolding of ES species and refolding by diluting freshly prepared 10 M urea stock solutions of ES species to the indicated concentrations of urea. These results demonstrate that the urea-induced unfolding transitions of ES species are reversible (data no shown), which is consistent with our previous report (*25*).

Tumor Inhibition and Tumor Blood Vessel Density Analysis. Animal studies followed the procedure described by Shi et al. (*21*) with modifications. C57BL/6 mice bearing Lewis lung carcinoma (LLC) were sacrificed at day 10 after nine daily subcutaneous injections at the indicated doses.

Statistical Methods. Data are expressed as means ± the standard deviation. Statistical significance was assessed by the one-tailed Student's *t* test. *P* values were obtained *via* comparison with indicated groups. *P* values of < 0.05 were considered statistically significant.

RESULTS

Identification of the N-Terminal Truncations of Endostatin Expressed by P. pastoris. The heterogeneity of endostatin expressed in *P. pastoris* (pES) was measured by SDS−PAGE, in which pES shows three bands on its reduced SDS−PAGE gel and two bands on its nonreduced SDS−PAGE gel (Figure 1A). To exclude contamination of pES as the cause of its heterogeneity, all bands were verified to be target proteins by Western blotting using an anti-endostatin monoclonal antibody (data not shown). Moreover, the nonreduced form has a faster mobility than the reduced form, which is due to the more compact globular structure caused by the two pairs of nested disulfide bonds (Figure 1A) (*29*−*31*). The heterogeneity of pES was further verified by reverse phase HPLC analysis, in which pES displays five peaks (Figure 1B). These results demonstrate that pES is heterogeneous with different molecular weights and varieties of conformations.

To identify individual variants of pES, each peak of pES was collected and was subjected to N-terminal sequencing. The relative amount of each peak determined by the HPLC profile and the relative intensity of the N-terminal sequencing signals were used to calculate the relative abundance of each individual component. Table 1 shows that in addition to the full-length endostatin, which occupies only 5% of the total pES protein, four other components were also detected: Y-full-length endostatin (Y is from expression vector pPIC9K of *P. pastoris*), endostatin lacking the first His residue (N-1), endostatin lacking the first three residues (HSH) (N-3), and endostatin lacking the first four residues (HSHR) (N-4). They occupy 26, 10, 22, and 35%, respectively, of the total pES protein. These four components all resulted from different N-terminal truncations of endostatin upon expression in *P. pastoris*. On the basis of the fact that there is no glycosylation site on the endostatin molecule, homogeneous recombinant protein samples of the wild-type endostatin (ES), N-1, N-3, and N-4 used in the subsequent investigation were constructed and expressed in *E. coli* to eliminate the difference in expression and isolation from different organisms (Figure 1C).

To determine the disulfide bond patterns in recombinant pES, ES, N-1, N-3, and N-4, MALDI TOF MS was employed. All protein samples were subjected to double enzymatic digestions with trypsin and chymotrypsin, and the molecular weights of the nonreduced and reduced digested fragments were measured. Two pairs of nested disulfide bonds (C33−C173 and C135−C165) were detected with all species tested (Table 2), while little mispairing patterns or free sulfhydryl groups were observed. These studies demonstrate that the disulfide bond patterns of endostatin and its variants from *E. coli* and *P. pastoris* not only are identical but also are consistent with the nested pattern of the two pairs of disulfide bonds in the native structure of endostatin revealed by crystallography (Figure 1D) (*11*).

Contributions of the N-Terminal Integrity to the Zinc Binding and Secondary Structure of Endostatin. Because amino acid residues H1, H3, H11, and D76 of endostatin are involved in binding with one zinc ion (*12*, *13*), N-terminally truncated endostatin lacking one or two of the four zinc-binding residues H1 and H3 are expected to lose zinc-binding capacity. In fact, the molar ratios of zinc ion to ES, N-1, N-3, and N-4 were measured to be 0.94:1, 0.92:1, 0.41:1, and 0.23:1, respectively (Figure 2A). These results are consistent with previous reports that endostatin lacking the first residue (H) and endostatin lacking the first four residues (HSHR) give zinc ion:endostatin molar ratios of 1:1 and 0.2:1, respectively (*3*, *13*), and the zinc-binding capacity of N-1 may be contributed by an alternative zinc-binding site for H1 (*13*). The nonintegral numbers of zinc ions bound for species N-3 and N-4 presumably reflect the weaker zinc-binding affinity for these two variants. With regard to zinc-binding, we introduce another endostatin derivative called ZBP-ES, which has an extra zinc-binding peptide (ZBP) engineered at the N-terminus of the wild-type endostatin. The disulfide bond pattern of ZBP-ES was verified to be identical with that of ES and its variants (Table 2). The molar ratio of zinc ion to ZBP-ES was measured to be 1.96:1 (Figure 2A).

Because zinc ion is one of the most abundant trace metals in the blood circulation of normal individuals (*32*), we thus investigated the conformations of ES and its variants in the presence of zinc ions for the sake of physiological relevance. In the presence of zinc ions, all species exhibit multiple secondary structures mainly consisting of β-strands and loops, as evidenced by their far-UV circular dichroism (CD) spectra between 190 and 250 nm (Figure 2B). Although ES, N-1, N-3, and N-4 do not exhibit the characteristic shape of an α-helix around 222 nm, their spectra between 200 and 210 nm suggest the existence of a certain amount of helical structure (Figure 2B). When the spectra between 190 and 200 nm are studied, it seems that ES has more loop structures, while ZBP-ES exhibits more helical structures than N-1, N-3, and N-4 (Figure 2B). In addition, N-1, N-3, and N-4 shared

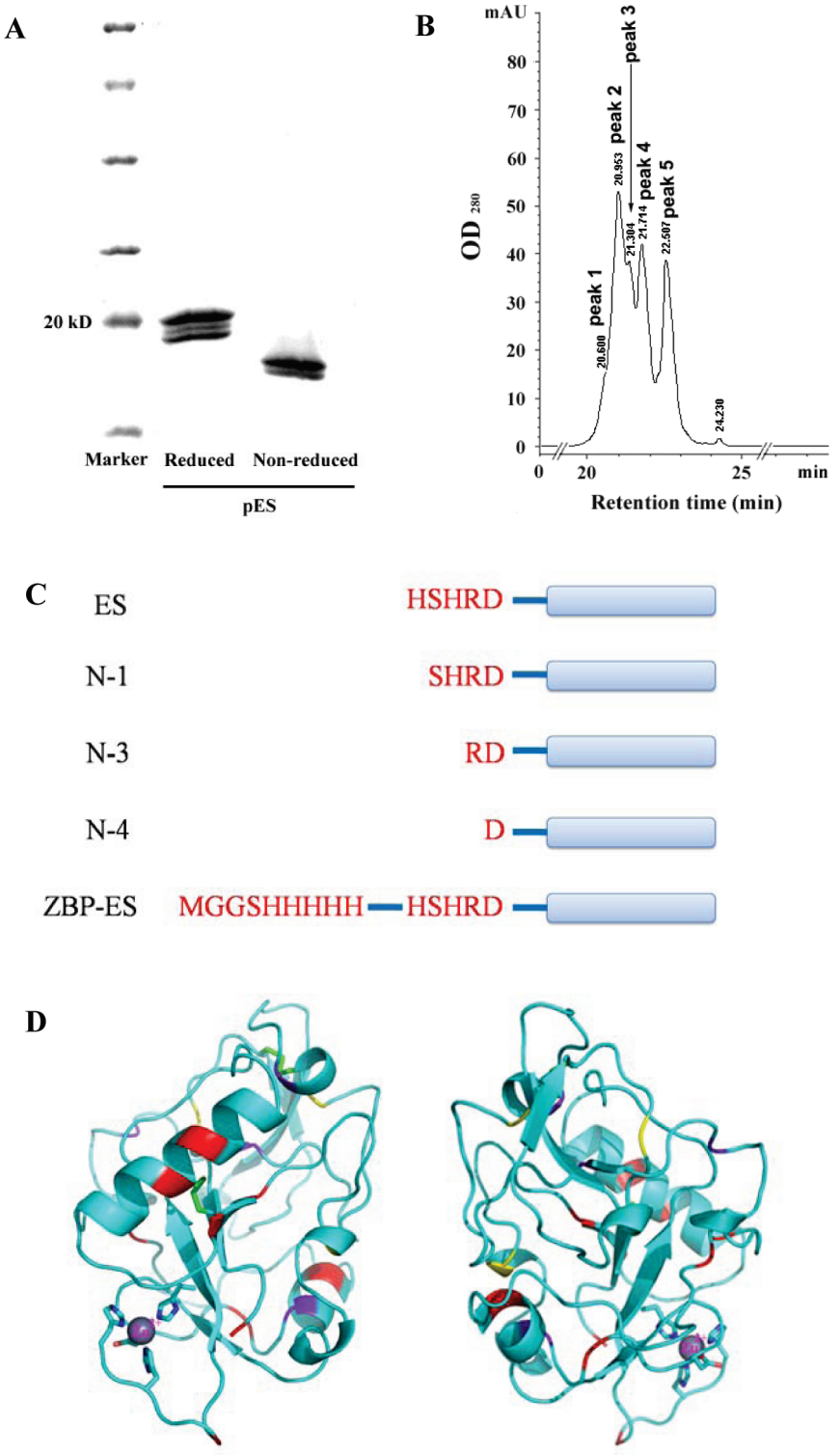

FIGURE 1: Identification of each species in pES. (A) SDS−PAGE profiles. Marker denotes molecular weight markers. (B) Reverse phase HPLC analysis of pES performed with an Agilent 1100 series instrument using a C_{18} reverse column. (C) Schematic drawing of the N-terminal sequences of ES, N-1, N-3, N-4, and ZBP-ES. (D) Three-dimensional structure of the endostatin molecule, illustrating the critical amino acid residues that contribute to the signals in tryptophan emission fluorescence and near-UV CD measurements. Red, yellow, and purple colors represent phenylalanine, tyrosine, and tryptophan residues, respectively, and the two pairs of disulfide bonds are colored green.

similar secondary structures, which are quite different from those of ES and ZBP-ES (Figure 2B).

Contributions of the N-Terminal Integrity to the Tertiary Structure of Endostatin. Because endostatin has four Trp amino acid residues spaced evenly throughout the molecule (Figure 1D), tryptophan emission fluorescence was used to monitor the tertiary structures of ES and its variants (*29*). In the presence of zinc ions, the maximal fluorescence emission wavelengths of all the species tested are around 320 nm (Figure 3A), which suggests that they all have compact tertiary structures (*29*, *31*). Moreover, ES, N-1, and ZBP-ES exhibit superimposed fluorescence spectra and share similar relative fluorescence intensities, which are evidently lower than those of N-3 and N-4 (Figure 3A). This observation indicates that the tertiary structures of ES, N-1, and

Table 1: Quantification and Identification of Each Component in pES by HPLC and N-Terminal Sequencing[a]

	peak 1 (7%)[b]		peak 2 (32%)[b]		peak 3 (13%)[b]		peak 4 (23%)[b]		peak 5 (25%)[b]		
component	% in peak 1	% in total pES	% in peak 2	% in total pES	% in peak 3	% in total pES	% in peak 4	% in total pES	% in peak 5	% in total pES	% in total pES
Y-full-length ES[c]	74	5	56	18	22	3	0	0	0	0	26
full-length ES	18	1	9	3	5	1	0	0	0	0	5
N-1[d]	5	0	15	5	37	5	0	0	0	0	10
N-3[e]	0	0	9	3	20	3	71	16	0	0	22
N-4[f]	0	0	4	1	12	2	29	7	100	25	35
others[g]	3	0	7	2	3	0	0	0	0	0	2

[a]Five peaks of pES (peaks 1−5) fractionated by reverse phase HPLC were subjected to N-terminal sequencing. The relative amount of each component of pES was identified and quantified. [b]The numbers in parentheses are the percentages of each peak in total pES based on reverse phase HPLC analysis. [c]Y (Tyr) is from expression vector pPIC9K of *P. pastoris*. [d]ES lacking the first H residue. [e]ES lacking the first three residues (HSH). [f]ES lacking the first four residues (HSHR). [g]Contaminant proteins copurified with pES.

Table 2: Summary of Disulfide Bond Pattern Identification[a]

protein	disulfide pair	(M + H) obsd	(M + H) calcd	δ
pES	C33−C173	1106.3857	1106.4521	−0.07
	C135−C165	2375.6400	2375.7383	−0.10
MES	C33−C173	1496.5200	1496.5904	−0.07
	C135−C165	1822.7354	1822.7468	−0.01
N-1	C33−C173	1106.3981	1106.4521	−0.05
	C135−C165	2375.6600	2375.7383	−0.08
N-3	C33−C173	1106.4203	1106.4521	−0.03
	C135−C165	2375.7400	2375.7383	0.00
N-4	C33−C173	1106.3955	1106.4521	−0.06
	C135−C165	2375.8300	2375.7383	0.09
ZBP-ES	C33−C173	1106.3867	1106.4521	−0.07
	C135−C165	2375.5200	2375.7383	−0.22

[a]Cys residues in all species are numbered according to the sequence of the wild-type endostatin.

ZBP-ES are more compact than those of N-3 and N-4 under the same conditions. Surprisingly, N-3 has the loosest tertiary structure among all the tested species (Figure 3A).

Because near-UV signals in the regions of 250−270, 270−290, and 280−300 nm can be attributed to phenylalanine, tyrosine, and tryptophan residues, respectively (*33*), and endostatin contains ten phenylalanine, three tyrosine, and four tryptophan residues (Figure 1D), near-UV CD was also employed to provide more information for the tertiary structure measurement. In the presence of zinc ions, all species share two major positive peaks around 250 and 280 nm, and one negative peak around 295 nm (Figure 3B). An only slight difference in the local structure around phenylalanine residues was observed with ES, N-1, N-4, and ZBP-ES, while the tertiary structure of N-3 is significantly different from those of the other four species (Figure 3B). These observations are largely consistent with the fluorescence study showing that truncation of the first three amino acid residues (HSH) at the N-terminus results in the most dramatic change in the tertiary structure compared with the other N-terminal truncations tested. It seems that a smaller difference is observed in the tertiary structures than in the secondary structures of ES and its variants. One possible explanation is that N-terminal truncations result in less significant changes in the overall tertiary structure than they do in the secondary structures. Another possibility is that the Trp fluorescence and near-UV CD studies reflect the local conformational changes in the tertiary structure around certain residues (Figure 3A,B), which would make some difference compared with the information of the secondary structures detected by CD (Figure 2B).

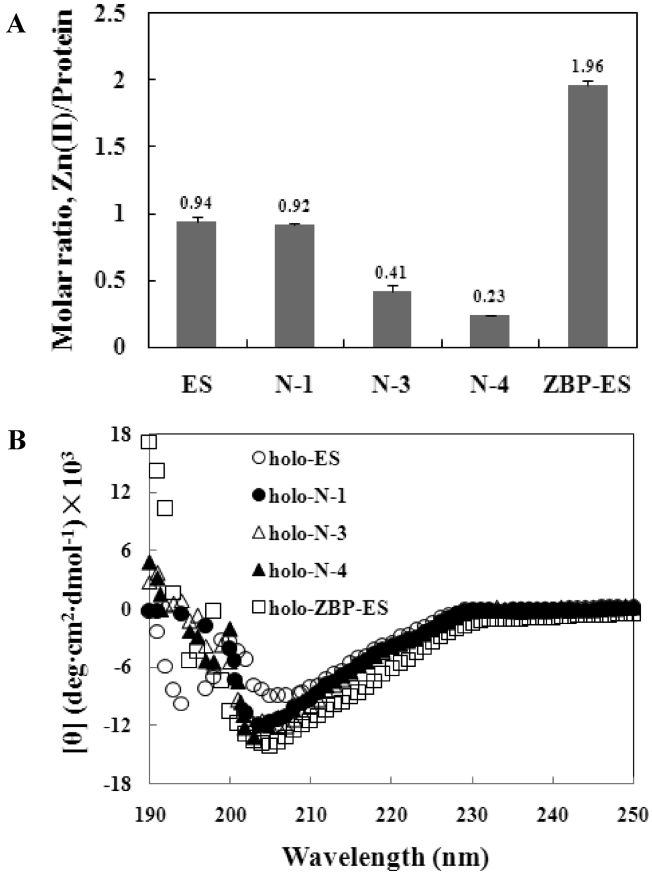

FIGURE 2: Zinc-binding capacities and secondary structures of ES, N-1, N-3, N-4, and ZBP-ES. (A) Molar ratios of Zn(II) to ES, N-1, N-3, N-4, and ZBP-ES. Error bars are standard deviations (n = 3). (B) Far-UV CD spectra of ES, N-1, N-3, N-4, and ZBP-ES detected in the presence of zinc ions. CD measurements were performed in 5 mM Tris-HCl containing 0.9% NaCl (pH 7.4) at 37 °C, and the protein concentrations were 10 μM. A 10-fold molar excess of $ZnCl_2$ was added, and a reference blank containing all reagents except protein served as a control.

In addition, to assess the overall compactness of the protein molecules, an AUC was employed. All the species show very good homogeneities of monomers with respect to size or mass as evidenced by the sedimentation coefficient distribution spectra collected at 60000 rpm (Figure 3C). The f/f_0 values of ES, N-1, N-3, N-4, and ZBP-ES were 1.335, 1.332, 1.413, 1.384, and 1.317, respectively. On the basis of the fact that the f/f_0 value of a protein provides an estimate of the extent to which the shape of a protein

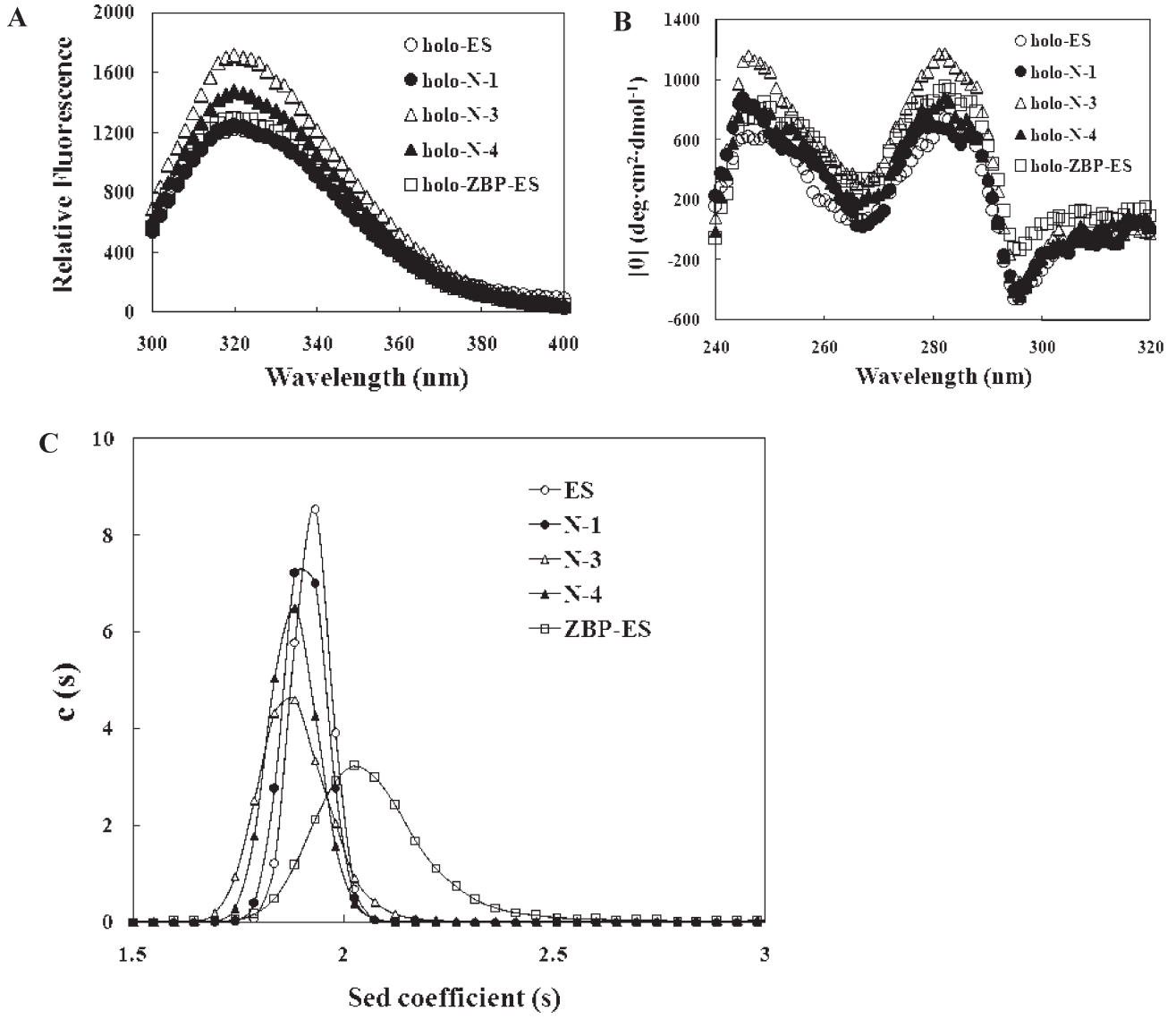

FIGURE 3: Tertiary structures of ES, N-1, N-3, N-4, and ZBP-ES in the presence of zinc ions. (A) Tryptophan emission fluorescence (FL) spectra for the holo forms of ES, N-1, N-3, N-4, and ZBP-ES. (B) Near-UV CD spectra for the holo forms of ES and its variants. All measurements were taken in 5 mM Tris-HCl containing 0.9% NaCl (pH 7.4) at 37 °C, and the protein concentrations for FL and CD measurements were 1 and 10 μM, respectively. A 10-fold molar excess of $ZnCl_2$ was added, and a reference blank containing all reagents except protein served as a control. (C) Sedimentation velocity analysis of ES, N-1, N-3, N-4, and ZBP-ES in the presence of zinc ions measured with an analytical ultracentrifuge (AUC). The f/f_0 values of ES, N-1, N-3, N-4, and ZBP-ES are 1.335, 1.332, 1.413, 1.384, and 1.317, respectively.

differs from a compact, unhydrated sphere of the same mass and density, and that the f/f_0 value for a globular protein gives a frictional coefficient of 1.2−1.4 (*34*, *35*), this result suggests that N-3 is the least compact while ZBP-ES has the most compact structure.

Contributions of the N-Terminal Integrity to the Structural Stability of Endostatin. Urea-induced unfolding was conducted in the presence of zinc to measure the thermodynamic stability and folding cooperativity of ES, N-terminally truncated endostatin, and ZBP-ES (Figure 4). The unfolding process was fitted and normalized according to the two-state model reported by Santoro and Bolen (*27*), which uses data both inside and outside the transition zone to fix the baselines. The free energy change (ΔG_{N-U}) of a protein was derived from the linear extrapolation of the transition zone between the native and unfolded states at the limit of a zero denaturant concentration (*27*). The concentrations of urea at the midpoint (C_m) of the unfolding transitions for holo-ES and holo-N-1 were measured to be 6.86 and 6.52 M, respectively, and the C_m values for holo-N-3 and holo-N-4 are much lower (Table 3). Because N-1 has a tertiary structure similar to that of ES, N-3 and N-4 have less compact structures than ES (Figure 3B,C), it is reasonable that when compared with ES, N-3 and N-4 show more dramatic decreases in thermodynamic stability than N-1 (Figure 4 and Table 3). Although the C_m value for holo-ZBP-ES (6.16 M) is lower than that of ES and N-1, the corresponding free energy change (ΔG_{N-U}) of holo-ZBP-ES (34.15 kJ/mol) is greater than those of holo-ES, holo-N-1, holo-N-3, and holo-N-4 (Table 3). These results demonstrate that holo-ZBP-ES is thermodynamically more stable than holo-ES and the N-terminally truncated endostatin proteins, and N-4 is the most unstable species (Table 3). Moreover, the apparent *m* values (slope or cooperativity of the unfolding curves) for holo-ES and holo-ZBP-ES are 4.37 and 5.54 kJ mol^{-1} M^{-1}, respectively, which suggests a much higher cooperativity of holo-ZBP-ES during the urea-induced unfolding process (Figure 4 and Table 3). Thus, it is reasonable to

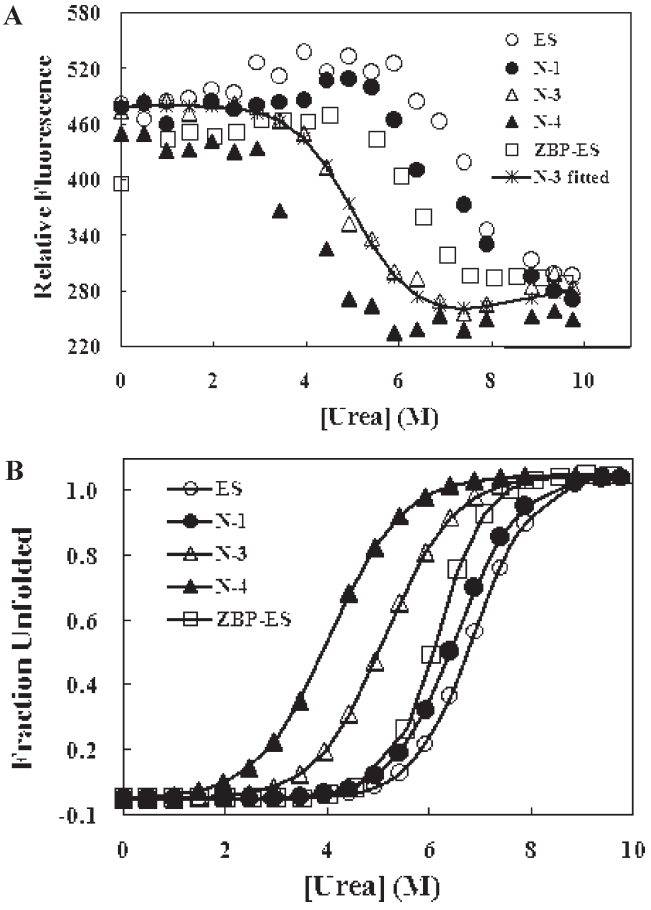

FIGURE 4: Contributions of the N-terminal integrity to the thermodynamic stability and folding cooperativity of endostatin against urea. The urea-induced unfolding processes of the holo forms of ES, N-1, N-3, N-4, and ZBP-ES were monitored by the tryptophan emission fluorescence at 318 nm. (A) Raw data and fitted curve. (B) Normalized curves. All measurements were taken in 5 mM Tris-HCl containing 0.9% NaCl (pH 7.4) at 37 °C, and the protein concentrations were 1 μM. A 10-fold molar excess of $ZnCl_2$ was added to ensure sufficient zinc-binding, and a reference blank at each concentration of urea containing all reagents except protein served as a control.

Table 3: Parameters of Urea-Induced Unfolding of ES, N-1, N-3, N-4, and ZBP-ES[a]

protein	ΔG_{N-U} (kJ mol^{-1})	m (kJ mol^{-1} M^{-1})	C_m (M)
ES	29.98	4.37	6.86
N-1	27.31	4.19	6.52
N-3	19.63	3.82	5.14
N-4	14.68	3.62	4.05
ZBP-ES	34.15	5.54	6.16

[a]Urea-induced unfolding of ES, N-1, N-3, N-4, and ZBP-ES was performed at 37 °C in the presence of zinc. The buffer was 0.9% NaCl in 5 mM Tris-HCl (pH 7.4). The unfolding curves of ES and its variants were fitted and normalized according to the procedure reported by Santoro and Bolen (*27*), which uses data both inside and outside the transition zone to fix the baselines. Urea-induced unfolding is reversible (see Materials and Methods for details). ΔG_{N-U}, the change of free energy in the absence of urea; m, the apparent m value defined by the linear extrapolation model; C_m, the concentration of urea at the midpoint of the unfolding transition.

speculate that the thermodynamic stability of pES is mainly contributed by the 31% pES components with an intact N-terminus [5% of ES and 26% of Y-ES (see Table 1)], because the N-terminally truncated forms of endostatin are much less stable.

In addition to the measurement of the thermodynamic stability, differential scanning calorimetry (DSC) was performed to measure the thermal stabilities of ES and its variants against heat. At least two conformational transition processes were observed with all the species tested, and no evident aggregation occurred even at 90 °C (data not shown). The midpoints of the first transition (T_m) of ES, N-1, N-3, N-4, and ZBP-ES are 56.6, 57.3, 55.6, 47.4, and 52.4 °C, respectively, among which ES, N-1, and N-3 do not show any significant difference (data not shown). It seems that the N-terminal integrity does not make contributions to the thermal stability of endostatin as dramatic as those it makes to the thermodynamic stability against urea, and the DSC thermogram may not be a suitable tool for the characterization of this protein. While the low stability of N-4 is expected, it is surprising that ZBP-ES shows less thermal stability than ES, N-1, and N-3 based on the T_m value, which is inconsistent with its thermodynamic stability in the urea-induced unfolding (Figure 4 and Table 3). A possible explanation for this inconsistency is that the heat-induced unfolding of the protein follows a mechanism different from that of urea-induced unfolding. Normally, urea can completely denature a protein by destroying both the hydrophobic interactions and the hydrogen bonds in a two-state reversible manner (*27*, *28*), while heat is more likely to denature protein molecules through a multistate process without complete exposure of the hydrophobic interiors of proteins (*36*).

Taken together, the N-terminal integrity is demonstrated to be very critical for the conformation and thermodynamic stability of endostatin, which in turn may have a profound effect on their biological functions.

Contributions of the N-Terminal Integrity to the Biological Functions of Endostatin. The biological functions of ES, N-terminally truncated endostatin, and ZBP-ES were tested both *in vitro* and *in vivo*. Human microvascular endothelial cell (HMEC) migration was used to evaluate the antiendothelial activities of ES and its variants. At a concentration of 160 μg/mL, ZBP-ES inhibits 57% of the HMEC migration, which shows the most potent efficacy among all the species tested at equal concentrations. The inhibitory effects of ES and N-1 (43 and 41%, respectively) are weaker than that of ZBP-ES. Only marginal inhibitory effects were observed with N-3 and N-4, which are 16 and 12%, respectively (Figure 5A).

Similar results were obtained in the Lewis lung carcinoma (LLC) mouse model. When ES, N-terminally truncated endostatin, and ZBP-ES were administered daily through subcutaneous injection at a dose of 4.5 mg/kg, ZBP-ES shows the most potent antitumor efficacy of 70% inhibition, which is higher than those of ES (64%), N-1 (57%), N-3 (23%), and N-4 (29%) based on the tumor weight analysis (Figure 5B).

Comparison between pES and ZBP-ES with Respect to the Antitumor and Antiangiogenic Efficacies. The main purpose of this study is to determine the contributions of N-terminal integrity to the stability and biological functions of endostatin; for this, we started from the endostatin expressed in *P. pastoris* (pES) consisting of varieties of N-terminally truncated forms. After systemic characterization of the contributions of different N-terminal sequences to the structural conformation, zinc-binding capacity, thermodynamic stability, and biological activities of endostatin, it becomes intriguing to evaluate the overall biological functions of pES, which are contributed by each species with different N-terminal sequences.

Because different doses of pES and ZBP-ES were tested in separate clinical trials on different tumor types and resulted in

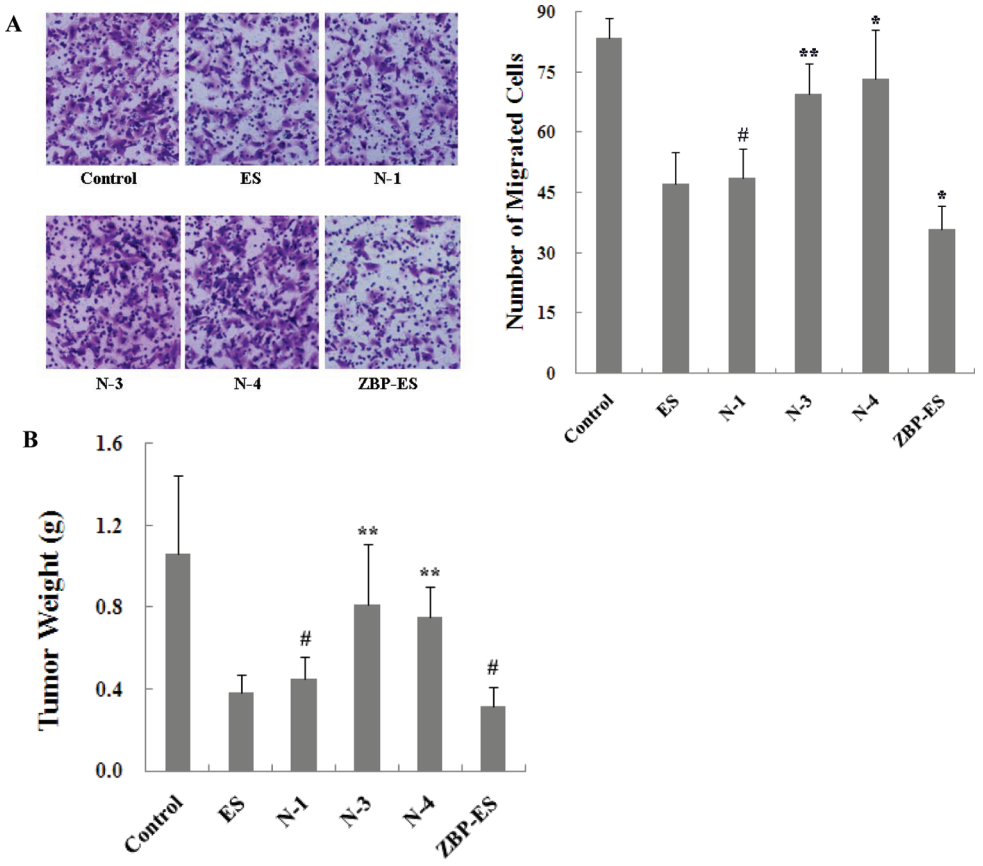

FIGURE 5: Comparison of the biological functions of ES, N-1, N-3, N-4, and ZBP-ES. (A) Comparison of the antiendothelial activity by a Transwell assay ($n = 6$). The left panel shows representative fields for each species, and the right panel shows quantified results. The protein concentration was 160 μg/mL, and saline served as a control. (B) Comparison of the antitumor activities in a Lewis lung carcinoma (LLC) mouse model ($n = 6$). ES, N-1, N-3, N-4, and ZBP-ES were subcutaneously injected daily into the C57BL/6 tumor-bearing mice at a dose of 4.5 mg/kg for 9 days. $p < 0.05$ (*), $p < 0.01$ (**), and $p > 0.05$ (#) *vs* the ES group. Error bars are standard deviations.

discrepant clinical outcomes (*4*, *10*, *16*, *17*, *20*), we took ZBP-ES to the parallel comparison with pES in their antitumor efficacies in the LLC animal model. pES and ZBP-ES at a dose of 1.5 mg/kg inhibit 19.4 and 45.3% of tumor growth, respectively, based on the tumor weight analysis (Figure 6). Moreover, pES and ZBP-ES inhibit 18.5 and 55% of tumor vascular growth, respectively (Figure 6), which correlates with the antitumor efficacies of pES and ZBP-ES.

DISCUSSION

Contributions of the N-Terminal Integrity and ZBP to the Conformation and Thermodynamic Stability of Endostatin. In this study, the N-terminally truncated forms of endostatin expressed in *P. pastoris* are identified to be N-1, N-3, and N-4. Truncations of different N-terminal amino acid residues result in quite different alterations in the properties of endostatin. Although N-1 lacks the first amino acid residue His and shows a similar zinc-binding capacity with ES (Figure 2A), it exhibits evident alterations in the secondary structure compared with ES (Figure 2B). Since it was reported that H1 can be replaced by the alternative zinc-binding site D5 (*13*), it is plausible that this alternative zinc coordination pattern contributes to such a change in the secondary structure. Interestingly, N-3 shows the least compact tertiary structure among all the species tested, which was evidenced by the Trp emission fluorescence, near-UV CD, and AUC studies (Figure 3). Because the N-terminus of a protein is positively charged and N-3 is the only molecule that starts with an amino acid residue (Arg) having a positively charged side chain among the species tested (Figure 1C), presumably the more extensive loss of structure of N-3 results from the unfavorable charge−charge repulsion at its N-terminus. In addition, ZBP-ES shows the most compact packing as evidenced by its lowest f/f_0 value (1.317) among all the ES variants tested (Figure 3C), which suggests that the conformation of ZBP-ES is somehow tightened by the extra zinc-binding.

The thermodynamic stability of endostatin against urea is evidently decreased by N-terminal truncations, while ZBP increases the cooperativity and thermodynamic stability of endostatin (Figure 4 and Table 3). It is plausible that the conformational changes caused by N-terminal truncations translate to the decreased thermodynamic stabilities of N-1, N-3, and N-4, and different conformations of these variants contribute to the differences in the relative stability of the molecules. A possible explanation for the higher cooperativity of holo-ZBP-ES is that upon the extra zinc-binding, holo-ZBP-ES is more tightly packed compared with the four other species as evidenced by its lowest f/f_0 value in the AUC study (Figure 3C), which endows the molecule with a higher cooperativity during urea-induced unfolding. Since it was reported that the cooperativity and thermodynamic stability are intimately linked (*28*), it is reasonable that ZBP-ES has a higher thermodynamic stability than ES and N-terminally truncated endostatin (Figure 4 and Table 3). In addition, the differences in the thermodynamic stability of ES and its variants caused by different N-terminal sequences correlate well with their biological activities (Figure 5).

In summary, keeping an intact N-terminus is very important for efficient zinc-binding and is essential for not only the structure

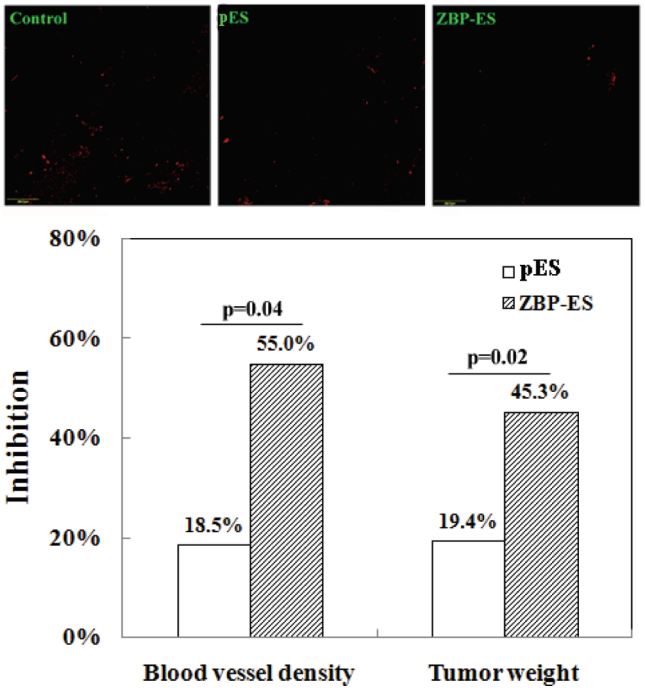

FIGURE 6: Comparison of the antitumor and antiangiogenic efficacies of pES and ZBP-ES. A tumor inhibition study of pES and ZBP-ES on LLC lung cancer was conducted with C57BL/6 mice ($n = 6$). pES and ZBP-ES were administered at 1.5 mg/kg for 9 days through subcutaneous daily injection. Tumor blood vessels (red) in the LLC model were detected by CD31 staining (top). Inhibition of the microvessel density and tumor weight were quantified (bottom).

and stability but also the biological functions of endostatin. In this regard, making the right endostatin molecule is the prerequisite for testing its efficacy, which has been largely ignored in previous studies.

Comparison of the Expression Systems for Endostatin Preparation. *E. coli* and *P. pastoris* are the two most commonly used expression systems for endostatin preparation (*1*−*3*, *5*, *20*). Upon expression in *E. coli*, endostatin forms inclusion bodies, which are inactive and highly insoluble under physiological conditions, and the refolding was reported to be extremely difficult (*1*). Because there is no glycosylation site on endostatin, *P. pastoris* was thus widely used to prepare soluble endostatin to avoid the refolding problem.

Although the antiangiogenic function of endostatin has been well accepted, controversial results generated with the samples prepared in different expression systems were reported for its antitumor activity (*7*, *9*, *37*). Intriguingly, complete regression of tumors with long-term microscopic dormancy has been observed only with recombinant endostatin expressed by *E. coli* (*1*, *6*, *38*, *39*). Here we show that pES is very heterogeneous with a variety of N-terminal truncations (Figure 1A,B and Table 1) and that the N-terminal integrity is very critical both for the thermodynamic stability and for the biological functions of endostatin (Figures 4 and 5). Moreover, the biological functions of pES reflect the overall contributions of endostatin and its truncated forms; the relative stability and activity of ES and its variants are quantitatively measured in this study. Although the heterogeneity of the *P. pastoris* expression varies from batch to batch (*40*), we observed that the overall HPLC profiles of pES remain similar during the period of this study. These results sufficiently explain the inconsistent antitumor activity of endostatin expressed in *P. pastoris*, which demonstrates that *P. pastoris* is not suitable for the preparation of proteins with critical sites at the N-terminus.

Although ZBP-ES appears to be more potent than pES in clinical trials (*4*, *10*, *17*, *18*, *20*), a head-to-head comparison between these two intimately related molecules is lacking, especially because different tumor types, doses, and drug delivery approaches were used. This study shows that the antiangiogenic and antitumor functions of ZBP-ES are significantly more potent than that of pES in animal models (Figure 6). In addition, an independent parallel study performed by Folkman and colleagues shows that ZBP-endostatin is at least twice as potent as pES in animal tumor models (*41*). Toward this end, our study reveals that pES has a variety of N-terminally truncated forms, which lost part of its zinc-binding site and becomes less potent than the wild-type ES. Moreover, when the wild-type ES and ZBP-ES are both expressed in *E. coli*, ZBP-ES shows a higher thermodynamic stability against urea and significantly more potent antiendothelial activity than ES (Table 3 and Figure 5A), although the difference between the antitumor activities of ZBP-ES and ES is not that significant (Figure 5B). Because pES, ES, N-1, N-3, N-4, and ZBP-ES are shown to have an identical disulfide bond pattern (Table 2), the loss of the N-terminal integrity of pES is quite possibly the major reason for the unmet clinical performance of endostatin expressed in *P. pastoris*.

Taken together, our study demonstrates that the N-terminal integrity is very critical for the stability and biological functions of endostatin and that the expression systems make a huge difference with respect to the properties of endostatin. These results provide fundamental explanations for the inconsistent antitumor activities of endostatin in a variety of studies, including the different therapeutic efficacies of endostatin and ZBP-endostatin in clinical trials.

ACKNOWLEDGMENT

We gratefully appreciate Tuo Zhang at Beijing Proteomics Research Centre for his technical assistance with the identification of disulfide bond patterns, Xiaoxia Yu at the Institute of Biophysics, Chinese Academy of Sciences, for technical assistance in AUC measurements, and Jingtan Su at Tsinghua University and Peng Liu at the National Engineering Laboratory for Antitumor Protein Therapeutics for their technical assistance with the DSC assay. We also appreciate all the members of the Luo laboratory for constructive suggestions and insightful discussions throughout this work, Bipo Sun for her lab routine management, and Protgen Ltd. for the generous gifts of the protein samples.

REFERENCES

1. O'Reilly, M. S., Boehm, T., Shing, Y., Fukai, N., Vasios, G., Lane, W. S., Flynn, E., Birkhead, J. R., Olsen, B. R., and Folkman, J. (1997) Endostatin: An endogenous inhibitor of angiogenesis and tumor growth. *Cell 88*, 277–285.
2. Sim, B. K., Fogler, W. E., Zhou, X. H., Liang, H., Madsen, J. W., Luu, K., O'Reilly, M. S., Tomaszewski, J. E., and Fortier, A. H. (1999) Zinc ligand-disrupted recombinant human endostatin: Potent inhibition of tumor growth, safety and pharmacokinetic profile. *Angiogenesis 3*, 41–51.
3. Boehm, T., O'Reilly, M. S., Keough, K., Shiloach, J., Shapiro, R., and Folkman, J. (1998) Zinc-binding of endostatin is essential for its antiangiogenic activity. *Biochem. Biophys. Res. Commun. 252*, 190–194.
4. Herbst, R. S., Hess, K. R., Tran, H. T., Tseng, J. E., Mullani, N. A., Charnsangavej, C., Madden, T., Davis, D. W., McConkey, D. J., O'Reilly, M. S., Ellis, L. M., Pluda, J., Hong, W. K., and Abbruzzese, J. L. (2002) Phase I study of recombinant human endostatin in patients with advanced solid tumors. *J. Clin. Oncol. 20*, 3792–3803.

5. Thomas, J. P., Arzoomanian, R. Z., Alberti, D., Marnocha, R., Lee, F., Friedl, A., Tutsch, K., Dresen, A., Geiger, P., Pluda, J., Fogler, W., Schiller, J. H., and Wilding, G. (2003) Phase I pharmacokinetic and pharmacodynamic study of recombinant human endostatin in patients with advanced solid tumors. *J. Clin. Oncol. 21*, 223–231.
6. Perletti, G., Concari, P., Giardini, R., Marras, E., Piccinini, F., Folkman, J., and Chen, L. (2000) Antitumor activity of endostatin against carcinogen-induced rat primary mammary tumors. *Cancer Res. 60*, 1793–1796.
7. Feldman, A. L., Alexander, H. R., Hewitt, S. M., Lorang, D., Thiruvathukal, C. E., Turner, E. M., and Libutti, S. K. (2001) Effect of retroviral endostatin gene transfer on subcutaneous and intraperitoneal growth of murine tumors. *J. Natl. Cancer Inst. 93*, 1014–1020.
8. Pawliuk, R., Bachelot, T., Zurkiya, O., Eriksson, A., Cao, Y. H., and Leboulch, P. (2002) Continuous intravascular secretion of endostatin in mice from transduced hematopoietic stem cells. *Mol. Ther. 5*, 345–351.
9. Marshall, E. (2002) Setbacks for endostatin. *Science 295*, 2198–2199.
10. Kulke, M. H., Bergsland, E. K., Ryan, D. P., Enzinger, P. C., Lynch, T. J., Zhu, A. X., Meyerhardt, J. A., Heymach, J. V., Fogler, W. E., Sidor, C., Michelini, A., Kinsella, K., Venook, A. P., and Fuchs, C. S. (2006) Phase II study of recombinant human endostatin in patients with advanced neuroendocrine tumors. *J. Clin. Oncol. 24*, 3555–3561.
11. Hohenester, E., Sasaki, T., Olsen, B. R., and Timpl, R. (1998) Crystal structure of the angiogenesis inhibitor endostatin at 1.5 angstrom resolution. *EMBO J. 17*, 1656–1664.
12. Ding, Y. H., Javaherian, K., Lo, K. M., Chopra, R., Boehm, T., Lanciotti, J., Harris, B. A., Li, Y., Shapiro, R., Hohenester, E., Timpl, R., Folkman, J., and Wiley, D. C. (1998) Zinc-dependent dimers observed in crystals of human endostatin. *Proc. Natl. Acad. Sci. U.S.A. 95*, 10443–10448.
13. Hohenester, E., Sasaki, T., Mann, K., and Timpl, R. (2000) Variable zinc coordination in endostatin. *J. Mol. Biol. 297*, 1–6.
14. Han, Q., Fu, Y., Zhou, H., He, Y. B., and Luo, Y. Z. (2007) Contributions of Zn(II)-binding to the structural stability of endostatin. *FEBS Lett. 581*, 3027–3032.
15. Tjin, R. M., Sjin, T., Satchi-Fainaro, R., Birsner, A. E., Ramanujam, V. M. S., Folkman, J., and Javaherian, K. (2005) A 27-amino-acid synthetic peptide corresponding to the NH2-terminal zinc-binding domain of endostatin is responsible for its antitumor activity. *Cancer Res. 65*, 3656–3663.
16. Eder, J. P., Supko, J. G., Clark, J. W., Puchalski, T. A., Garcia-Carbonero, R., Ryan, D. P., Shulman, L. N., Proper, J., Kirvan, M., Rattner, B., Connors, S., Keogan, M. T., Janicek, M. J., Fogler, W. E., Schnipper, L., Kinchla, N., Sidor, C., Phillips, E., Folkman, J., and Kufe, D. W. (2002) Phase I clinical trial of recombinant human endostatin administered as a short intravenous infusion repeated daily. *J. Clin. Oncol. 20*, 3772–3784.
17. Yang, L., Wang, J., Tang, Z., Liu, X., Huang, J., Li, S., Dong, Y., Zhang, H., Xue, L., Chu, D., and Sun, Y. (2004) A phase I clinical trial for recombinant human endostatin. *Zhongguo Xinyao Zazhi 13*, 6.
18. Yang, L., Jinwan, W., Yan, S., Yunzhong, Z., Liu, X., Li, W., Di, L., Li, P., Wang, Y., Song, S., Yao, C., and You, L. (2006) Randomized Phase II trial on escalated doses of Rh-endostatin (YH-16) for advanced non-small cell lung cancer. *Chin. J. Oncol. 28*, 4.
19. Yang, L., Wang, J. W., Cui, C., Huang, J., Zhang, H., Li, S., and Sun, Y. (2005) Rh-endostatin (YH-16) in combination with vinorelbine and cisplatin for advanced non-small cell lung cancer: A multicenter phase II trial. *Zhongguo Xinyao Zazhi 14*, 4.
20. Wang, J. W., Sun, Y., Liu, Y., Yu, Q., Zhang, Y., Li, K., and Zhu, Y. (2005) Results of randomized, multicenter, double-blind phase III trial of rh-endostatin (YH-16) in treatment of advanced non-small cell lung cancer patients. *Zhongguo Feiai Zazhi 8*, 8.
21. Shi, H. B., Huang, Y. J., Zhou, H., Song, X. M., Yuan, S. P., Fu, Y., and Luo, Y. Z. (2007) Nucleolin is a receptor that mediates antiangiogenic and antitumor activity of endostatin. *Blood 110*, 2899–2906.
22. Huang, Y. J., Shi, H. B., Zhou, H., Song, X. M., Yuan, S. P., and Luo, Y. Z. (2006) The angiogenic function of nucleolin is mediated by vascular endothelial growth factor and nonmuscle myosin. *Blood 107*, 3564–3571.
23. Ades, E. W., Candal, F. J., Swerlick, R. A., George, V. G., Summers, S., Bosse, D. C., and Lawley, T. J. (1992) HMEC-1: Establishment of an immortalized human microvascular endothelial cell line. *J. Invest. Dermatol. 99*, 683–690.
24. Edelhoch, H. (1967) Spectroscopic determination of tryptophan and tyrosine in proteins. *Biochemistry 6*, 1948–1954.
25. Fu, Y., Wu, X., Han, Q., Liang, Y., He, Y., and Luo, Y. (2008) Sulfate stabilizes the folding intermediate more than the native structure of endostatin. *Arch. Biochem. Biophys. 471*, 232–239.
26. Fu, Y., Chen, Y., Luo, X., Liang, Y., Shi, H. B., Gao, L., Zhan, S. L., Zhou, D. F., and Luo, Y. Z. (2009) The Heparin Binding Motif of Endostatin Mediates Its Interaction with Receptor Nucleolin. *Biochemistry 48*, 11655–11663.
27. Santoro, M. M., and Bolen, D. W. (1988) Unfolding free energy changes determined by the linear extrapolation method. 1. Unfolding of phenylmethanesulfonyl α-chymotrypsin using different denaturants. *Biochemistry 27*, 8063–8068.
28. Luo, Y., Kay, M. S., and Baldwin, R. L. (1997) Cooperativity of folding of the apomyoglobin pH 4 intermediate studied by glycine and proline mutations. *Nat. Struct. Biol. 4*, 925–930.
29. Li, B., Wu, X. Y., Zhou, H., Chen, Q. J., and Luo, Y. Z. (2004) Acid-induced unfolding mechanism of recombinant human endostatin. *Biochemistry 43*, 2550–2557.
30. Wu, X. Y., Huang, J., Chang, G. D., and Luo, Y. Z. (2004) Detection and characterization of an acid-induced folding intermediate of endostatin. *Biochem. Biophys. Res. Commun. 320*, 973–978.
31. Zhou, H., Wang, W., and Luo, Y. Z. (2005) Contributions of disulfide bonds in a nested pattern to the structure, stability, and biological functions of endostatin. *J. Biol. Chem. 280*, 11303–11312.
32. Ogunlewe, J. O., and Osegbe, D. N. (1989) Zinc and cadmium concentrations in indigenous blacks with normal, hypertrophic, and malignant prostate. *Cancer 63*, 1388–1392.
33. Santucci, R., Ascoli, F., Amiconi, G., Bertollini, A., and Brunori, M. (1985) Conformational-Changes Induced by Polyanions in Hemoglobin from *Camelus dromedarius*: Circular-Dichroism Study on the Oxy Derivative. *Biochem. J. 231*, 793–796.
34. Lelj-Garolla, B., and Mauk, A. G. (2006) Self-association and chaperone activity of Hsp27 are thermally activated. *J. Biol. Chem. 281*, 8169–8174.
35. Lebowitz, J., Lewis, M. S., and Schuck, P. (2002) Modern analytical ultracentrifugation in protein science: A tutorial review. *Protein Sci. 11*, 2067–2079.
36. Gloss, L. M., and Matthews, C. R. (1997) Urea and thermal equilibrium denaturation studies on the dimerization domain of *Escherichia coli* Trp repressor. *Biochemistry 36*, 5612–5623.
37. Celik, I., Surucu, O., Dietz, C., Heymach, J. V., Force, J., Hoschele, I., Becker, C. M., Folkman, J., and Kisker, O. (2005) Therapeutic efficacy of endostatin exhibits a biphasic dose-response curve. *Cancer Res. 65*, 11044–11050.
38. Boehm, T., Folkman, J., Browder, T., and OReilly, M. S. (1997) Antiangiogenic therapy of experimental cancer does not induce acquired drug resistance. *Nature 390*, 404–407.
39. Huang, X., Wong, M. K., Zhao, Q., Zhu, Z., Wang, K. Z., Huang, N., Ye, C., Gorelik, E., and Li, M. (2001) Soluble recombinant endostatin purified from *Escherichia coli*: Antiangiogenic activity and antitumor effect. *Cancer Res. 61*, 478–481.
40. Toonkool, P., Metheenukul, P., Sujiwattanarat, P., Paiboon, P., Tongtubtim, N., Ketudat-Cairns, M., Ketudat-Cairns, J., and Svasti, J. (2006) Expression and purification of dalcochinase, a β-glucosidase from *Dalbergia cochinchinensis* Pierre, in yeast and bacterial hosts. *Protein Expression Purif. 48*, 195–204.
41. Jia, H., and Kling, J. (2006) China offers alternative gateway for experimental drugs. *Nat. Biotechnol. 24*, 117–118.